

Gate-Defined Quantum Dots on Carbon Nanotubes

M. J. Biercuk, S. Garaj, N. Mason, J. M. Chow, C. M. Marcus

Department of Physics, Harvard University

Cambridge, MA 02138

We report the realization of nanotube-based quantum dot structures that use local electrostatic gating to produce individually controllable dots in series along a nanotube. Electrostatic top-gates produce depletion regions in the underlying tube; a pair of such depletion regions defines a quantum dot. Transparencies of tunnel barriers as well as the electrostatic energies, within single and multiple dots, can be tuned by gate voltages. The approach allows accurate control over multiple devices on a single tube, and serves as a design paradigm for nanotube-based electronics and quantum systems.

A number of proposed solid-state quantum devices [1] take as their fundamental element the quantum dot—a classically isolated island of electrons with a discrete energy spectrum [1, 2]. The discovery of carbon nanotubes [3], and subsequent study of their unique electrical and mechanical properties [4], suggests the use of these materials for fundamental studies of 1D physical systems [5] and as alternatives to semiconductor heterostructures for the fabrication of quantum-dot-based electrical devices, including physical qubits for encoding quantum states of spin or charge. To date, however, these investigations [6-9] have been limited by the difficulty of fabricating multiple or complex devices on a single tube.

In previous studies, isolated quantum dots formed in carbon nanotubes are formed either by tunnel barriers at the metal-nanotube interface [4, 10], or by intrinsic [7, 11] or induced [12, 13] defects along the tube. These devices have demonstrated the potential of nanotube-based quantum devices, but have suffered from a lack of independent control over device parameters (e.g., charge number and tunnel barrier transparency) as well as stringent geometric constraints on device design. In the present study, we instead rely on

lithographically defined gates and transparent contacts to the nanotube. This design allows the formation of single or multiple intratube quantum dots arbitrarily positioned along a tube (quantum dots connected to 1D nanotube leads), with independent control over tunnel barriers and dot charges. A backgate is used to reduce intrinsic scattering due to impurities and defects along the nanotube and to set overall carrier density.

Nanotubes were grown via chemical vapor deposition from lithographically defined Fe catalyst islands on a degenerately doped Si wafer with 1 μ m of thermally grown oxide (See Fig. 1a). Atomic force microscopy was used to locate nanotubes relative to alignment markers, and single walled tubes with diameters less than ~ 3 nm were contacted with 15 nm of Pd, patterned by electron beam lithography [14]. Device lengths were in the range 5–25 μ m. After contacting, the entire sample was coated with 25–35 nm of either SiO₂ deposited by plasma-enhanced chemical vapor deposition (PECVD) or Al₂O₃ deposited by atomic layer deposition (ALD). Cr/Au top-gates, 150–300 nm wide, were then patterned over the tubes using electron-beam lithography, with care taken to prevent overlap between the gates and the Pd contacts.

Two-terminal conductance was measured in either a pumped ⁴He cryostat (300K to 1.5K) or a ³He cryostat (300K to 0.3K). Current and differential conductance, dI/dV , were measured simultaneously using a combined ac + dc voltage bias with a current amplifier (Ithaco 1211) and lockin amplifier.

All semiconducting nanotubes coated with PECVD SiO₂ showed p-type field effect transistor behavior at room-temperature, exhibiting carrier depletion with positive voltage applied to top or back-gates (hence a suppression of conductance by three to four orders of magnitude at voltages of ~ 1 –3V) [15]. In contrast, many tubes with ALD

showed n-type or ambipolar behavior (high conductance at either positive or negative applied top or back-gate voltage surrounding a low-conductance region) with thermally activated conductance in the gap. Room-temperature maximum conductances at zero dc bias, $V_{SD}=0$, ranged from $\sim 0.5 - 2 e^2/h$. Devices showing a weak gate response (presumably metallic) were not investigated further.

Single quantum dots were formed using an effective three-gate configuration (Fig. 1a), where outer gates act as tunnel barriers defining the dot (denoted “barrier 1” and “barrier 2”) by locally depleting carriers beneath them, and a center gate (denoted “plunger”) shifts the chemical potential in the dot relative the chemical potentials of the contacts and the segments of the tube away from the gates. Gate response of tube conductance for a single-dot device using PECVD SiO_2 (micrograph of similar device shown in Fig. 1b, inset; the two center gates connected and act as one plunger gate) shows p-type field effect behavior, that is, the tube is depleted when gate bias becomes sufficiently positive. The gated region of the nanotube is $\sim 2 \mu\text{m}$ in length, while the total tube length is $\sim 25 \mu\text{m}$ between the Pd contacts (this device uses SiO_2 as a gate dielectric).

The independent action of the barrier gates is evident in the two-dimensional plot of differential conductance dI/dV as a function of barrier gate voltages, shown in Fig. 2a. The square edge of the conducting region demonstrates independent barrier depletion with little cross-coupling. Parallel diagonal features separated by $\sim 2 \text{ mV}$ evident near the pinch-off of both barrier gates (Fig. 2b) are a signature of Coulomb blockade, discussed below. Figure 2b demonstrates that adjusting the barrier gate voltages allows the full

transition from open conduction to weak tunneling through a gate-defined quantum dot—with well-defined Coulomb blockade peaks—to be controllably realized.

Examined as a function source-drain voltage bias, V_{SD} , as well as plunger gate voltage, the Coulomb blockade peaks form a series of repeated “Coulomb diamonds” where conduction is suppressed whenever the energy to add the next hole to the device exceeds V_{SD} (Fig. 2c). The ratio, $\eta^{-1} \sim 0.85$, of Coulomb diamond height (V_{SD}) to width (plunger voltage) gives the conversion $e\eta$ from the distance in plunger voltage between Coulomb blockade peaks to dot charging energy $E_C = e^2 / C \sim e^2 / \kappa\epsilon_0 L$ ($\kappa \sim 4$ is the dielectric constant of SiO_2), and indicates strong coupling of the plunger gate to the single-particle levels of the dot [6]. From this analysis, one extracts a dot length of $L \sim 2 \mu\text{m}$, which is roughly comparable to the size of the gated region of the tube, and much less than the $\sim 25 \mu\text{m}$ tube length. Several hundred consecutive Coulomb peaks are visible over a range of plunger gate voltage $> 4\text{V}$. Throughout this range, peak heights remain controllable by adjusting the barrier gates.

The data in Fig. 2c show significant off-resonance tunneling outside of the Coulomb diamonds, obscuring any excited state features that one would otherwise expect in low-temperature transport. This washing out of transport features is characteristic of the devices made with PECVD SiO_2 but is not the case for ALD Al_2O_3 , where excited state features are often visible outside the Coulomb diamonds. We do not know if this difference is due to the oxide material itself or due to damage that occurs during deposition. Figure 3 show a series of Coulomb diamonds measured on a gate-defined quantum dot using ALD Al_2O_3 as an insulating layer. Off-resonance conductance is low, and excited states are visible outside of the boundaries of the diamonds. The mean level

spacing extracted from the data $\Delta E = \hbar v_F / 2L \sim 2\text{-}3 \text{ mV}$ gives a measure of dot length, $L \sim 0.5\text{-}0.8 \text{ }\mu\text{m}$, again consistent with the lithographic dimensions of the gated region of the tube.

Taking advantage of the versatility of gate-defined devices, we next investigate a double quantum dot formed by three depletion regions along a nanotube. The double quantum dot, shown in Fig. 4a, comprises left and right barrier gates, a middle barrier gate and a two independent plunger gates. Gates are approximately 150 nm wide with 150 nm spacing; total nanotube length is $\sim 10 \text{ }\mu\text{m}$, much longer than the double dot.

Resonant transport through double dots in series occurs only when available energy levels in each dot align with each other and with the chemical potentials in the two leads [16]. When the mutual capacitance of the dots is weak, the alignment condition occurs at the intersection of the Coulomb peaks leading to a rectangular grid of resonant conduction peaks. Such a pattern is seen in Fig. 4(b). The resulting charge stability diagram is comprised of individual, approximately square cells, each of which corresponds to a well-defined charge number in both dots. Cross-coupling of plunger gates, which would skew the square pattern into rhombus shapes, appears to be quite small. We note that these measurements were conducted at $T \sim 1.5\text{K}$, higher than the typical temperature where double dots based on semiconductor heterostructures have been measured [16].

Increasing the coupling between the two dots (accomplished experimentally by reducing the voltage on the middle gate) leads to a splitting of the high-conductance points of degeneracy between different charge configurations, and the emergence of a honeycomb pattern in the charge stability diagram (Fig. 4c). The interdot interaction may

be due to capacitive or tunnel-coupling, but it has been shown that tunnel-coupling increases exponentially faster with a reduction of the interdot barrier [17]. In addition, as the voltage on the middle gate is reduced we observe an increase in vertex height by approximately an order of magnitude. It is therefore likely that finite tunnel coupling leads to the splitting of the vertices [18, 19] in Fig. 4c, which in this case is partially obscured by thermal broadening. (Any splitting of the charge degeneracy points in Fig. 4b is smaller than the thermal smearing.) In addition to the vertex splitting in Fig. 4c, we observe strong conductance along the edges of the honeycomb cells, due to higher-order processes through virtual states. Further decreasing the voltage on the middle gate yields a series of straight diagonal lines as a function of the two plunger gates as expected when the two dots merge to form a single large dot. The lines arise from Coulomb charging where both gates act additively in coupling to the single particle states of the dot (Fig. 4d) [20]. An analysis of the spacing between the Coulomb peaks along the total energy axis (a line perpendicular to the sloped lines) shows that the peak spacing in Fig. 4d, 4.8 mV, is half of that required to move from one degeneracy point to the next along a similar line in Fig. 4b, 9.6 mV. This factor of two corresponds nearly exactly to the difference in the size of a single dot between the isolated and strongly coupled cases for this device, as peak spacing is inversely proportional to dot length [4]. The fact that a single dot can be formed by outside barriers, with three nominally inactive gates between them suggests that there is little inadvertent depletion or tube damage from the deposition of these top gates.

An analysis of the total conductance through the double dot for different values of middle gate voltage is consistent with the interpretation that the interaction between the two dots is due to tunnel coupling. If we assume that tunneling rates through the barrier gates, Γ_{BL} and Γ_{BR} , are equal and remain roughly constant in the three coupling regimes we can relate the tunneling rates to the peak current for the single dot case as $I_p \sim 80 \text{ pA} = 2e \Gamma_{BL} \Gamma_{BR} / (\Gamma_{BL} + \Gamma_{BR})$ to find $\Gamma_{BL} = \Gamma_{BR} = \Gamma \sim 5 \text{ GHz}$. Using these values we solve for the middle barrier tunnel rate, Γ_M , from the peak current in the weak ($I_p \sim 5 \text{ pA}$) and intermediate ($I_p \sim 60 \text{ pA}$) coupling cases using $\Gamma_M^2 = I_p \Gamma^2 / 4(2e\Gamma - 3I_p)$ [16]. We find that for the weak coupling case $\Gamma_M \sim 100 \text{ MHz}$ and for intermediate coupling $\Gamma_M \sim 800 \text{ MHz}$, consistent with a modest visible splitting of the vertices for intermediate coupling. Finally, if we assume that in the weak coupling case tunneling through the middle barrier provides the dominant component of resistance, setting $\Gamma_M = I_p / e$ gives $\Gamma_M \sim 30 \text{ MHz}$, comparable to the value of 100 MHz obtained above.

We find that the ability to control via gates the transition from the open conduction to Coulomb charging regimes is quite reproducible, and has been investigated in eight devices with varying gate dimensions, configurations, and dot sizes. Double quantum dot devices have been investigated using both SiO_2 and Al_2O_3 , and again off-resonant conduction is reduced in double dots fabricated with Al_2O_3 as a gate oxide relative to those using SiO_2 . In addition, structure is visible inside the honeycomb vertex triangles for Al_2O_3 devices when measured at finite V_{SD} [21].

Looking forward, the recent realization [22] of centimeter-scale single-wall nanotubes makes possible the goal of fabricating hundreds of independently controlled quantum dots on a single nanotube. Controlled gating at arbitrary points along the tube

greatly enhances the functionality of nanotube devices for potential applications ranging from bucket brigade devices [23] to quantum coherent logic elements. This approach may be particularly useful for quantum logic, as recent theoretical work has shown that a one-dimensional array of coupled quantum dots can be used for quantum computation [24, 25]. Further, the expected long spin coherence lifetime [26] for electrons and holes in nanotubes makes this an attractive material for developing spin-based quantum information storage and processing systems.

This work was supported by ARO/ARDA (DAAD19-02-1-0039 and -0191), NSF-NIRT (EIA-0210736), and Harvard CIMS. M.J.B. acknowledges support from an NSF graduate research fellowship and an ARO-QCGR fellowship. S. G. acknowledges support from Bourse de Recherche, Swiss National Science Foundation. N. M. acknowledges support from the Harvard Society of Fellows.

References:

- [1] C. W. J. Beenakker and H. van Houten, in *Solid State Physics - Advances in Research and Applications*, edited by H. Ehrenreich, Turnbull, D. (Academic Press, San Diego, CA, 1991), Vol. 44, p. 1.
- [2] L. Kouwenhoven and C. Marcus, *Physics World* **11**, 35 (1998).
- [3] S. Iijima, *Nature* **354**, 56 (1991).
- [4] P. L. McEuen, et al., *Phys. Rev. Lett.* **83**, 5098 (1999).
- [5] M. Bockrath, et al., *Nature* **397**, 598 (1999).
- [6] M. Bockrath, et al. *Science* **275**, 1922 (1997).
- [7] M. Bockrath, et al. *Science* **291**, 283 (2001).
- [8] W. Liang, M. Bockrath, and H. Park, *Phys. Rev. Lett.* **88**, 126801 (2002).
- [9] M. R. Buitelaar, *Phys. Rev. Lett.* **91**, 057005 (2003).
- [10] J. Nygard, D. H. Cobden, and P. E. Lindelof, *Nature* **408**, 342 (2000).
- [11] N. Mason, M. J. Biercuk, and C. M. Marcus, *Science* **303**, 655 (2004).
- [12] H. W. C. Postma, et al. *Science* **293**, 76 (2001).
- [13] M. J. Biercuk, N. Mason, and C. M. Marcus, *Nano Lett.* **4**, 2499 (2004).
- [14] A. Javey, et al. *Nature* **424**, 654 (2003).
- [15] M. J. Biercuk, et al., *Phys. Rev. Lett.* **94** 026801 (2005).
- [16] W. G. van der Wiel, et al., *Rev. of Mod. Phys.* **75**, 1 (2003).
- [17] L. L. Sohn, L. Kouwenhoven, G. Schon, Editors *NATO ASI series. Series E, Applied Sciences* (Kluwer Academic Publishers, Boston, MA, 1997), Vol. 345.
- [18] F. R. Waugh, et al., *Physical Review Letters* **75**, 705 (1995).
- [19] C. Livermore, et al., *Science* **274**, 1332 (1996).
- [20] C. H. Crouch, et al., *Surface Science* **361-362**, 631 (1996).
- [21] To be published.
- [22] L. X. Zheng, et al., *Nature Mat.* **3**, 673 (2004).
- [23] See e.g. EG&G Reticon-RD5108
- [24] D. Loss and D. P. DiVincenzo, *Phys. Rev. A* **57**, 120 (1998).
- [25] G. Burkard, D. Loss, and D. P. DiVincenzo, *Phys. Rev. B* **59**, 2070 (1999).
- [26] L. Forro, Salvétat, J.-P., Bonard, J.-M., Bacsá, R., Thomson, N. H., Garaj, S., Thien-Nga, L., Gaal, R., Kulik, A., Ruzicka, B., Degiorgi, L., Bachtold, A., Schonenberger, C., Pekker, S., Hernadi, K., in *Science and Application of Nanotubes*, edited by D. Tomanek, Enbody, R. J. (Kluwer Academic/Plenum Publishers, New York, 2000), p. 297.

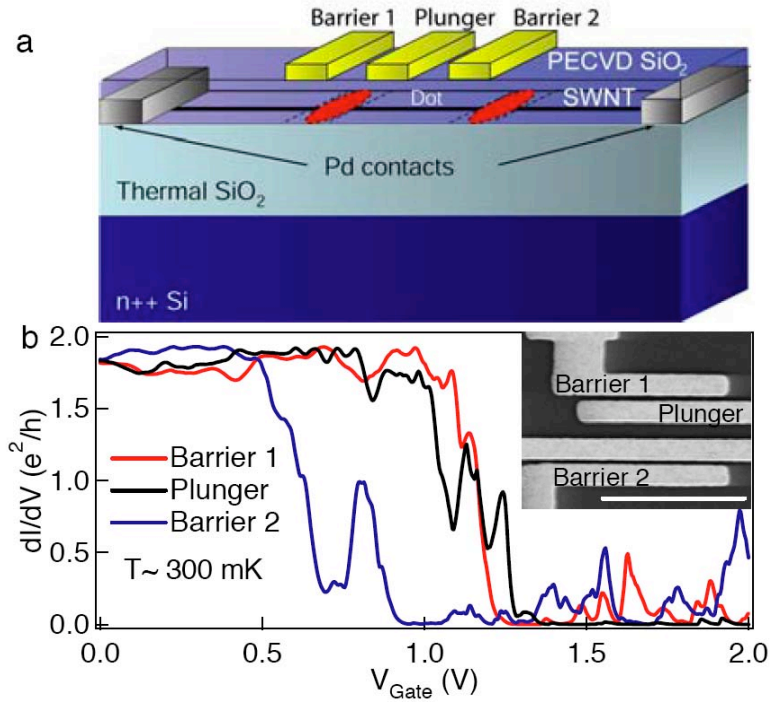


Figure 1a. Schematic of a gate-defined carbon nanotube quantum dot showing vertically integrated geometry and ohmic contacts. The use of Pd contacts in this study is imperative as no tunnel barrier is formed at the metal-nanotube interface.

1b. Low-temperature gate response of a $\sim 25 \mu\text{m}$ long nanotube contacted by Pd electrodes and top-gated using PECVD SiO_2 . Lockin excitation $\sim 10 \mu\text{V}$. For this device, all gates strongly suppress conductance at voltages above $\sim 1\text{V}$. Inset: SEM of a lithographically similar gate pattern. The middle two gates are connected together and serve as a single plunger gate. Scale bar = $2 \mu\text{m}$.

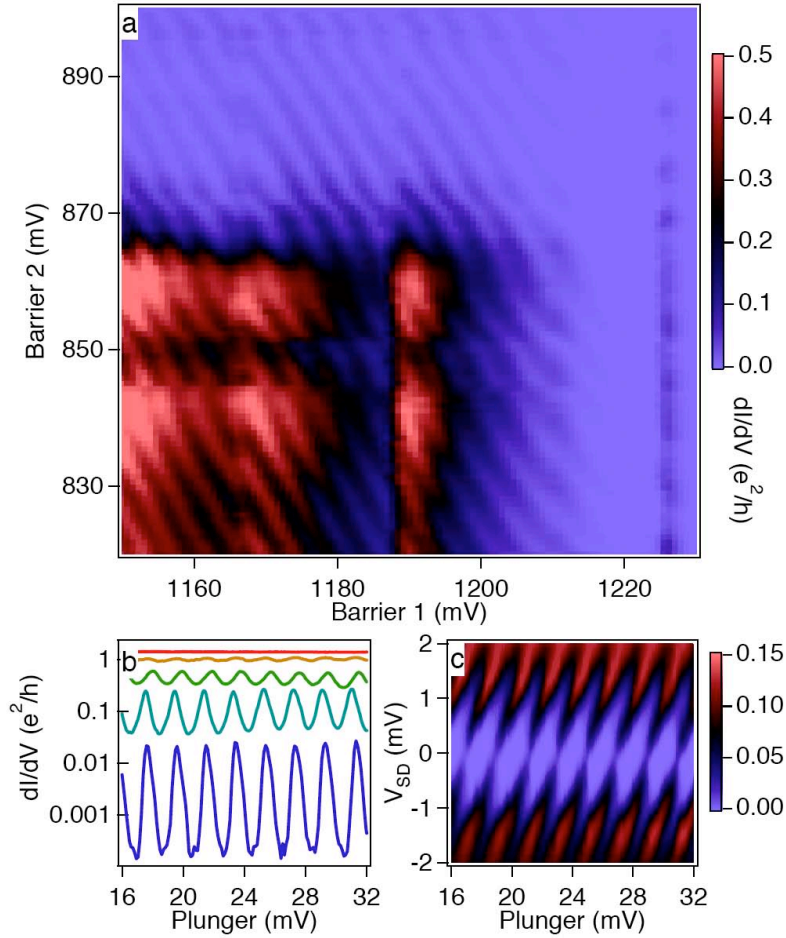


Figure 2a. Differential conductance, dI/dV , plotted as a function of barrier gate voltages. Conductance can be suppressed by the application of either gate voltage, leading to the observed corner. Both barrier gates couple capacitively to the carrier densities in the proximal sections of the nanotube and also to the chemical potential of the dot formed between the depletion regions. Thus, near full pinch-off with both gates we observe the emergence of a series of diagonal lines in the 2D plot due to the onset of single electron charging.

2b. dI/dV , on a logarithmic scale as a function of the plunger gate for various values of barrier gate voltages. Data measured on a subsequent cool down from those in panels a and c, where the exact position of the corner has shifted slightly in gate voltage. From bottom to top data are taken at various barrier gate values falling along a diagonal line (with slope approximately 0.8 in the Barrier 1 – Barrier 2 plane) starting from the corner at which conductance is pinched off towards lower gate voltages where conductance is larger. At the highest barrier gate voltages we measured isolated Coulomb blockade peaks where there is a degeneracy between subsequent charge states on the quantum dot defined by barrier gates. Decreasing the barrier gate voltages allows the controllable transition from isolated Coulomb blockade, through Coulomb oscillations on a

high conductance background, to open transport without any single electron charging effects apparent.

2c. Differential conductance, dI/dV , (in units of e^2/h) as a function of plunger gate voltage and source-drain voltage, V_{SD} , for Barrier 1 = 1200 mV and Barrier 2 = 880 mV. Coulomb diamonds represent regions of suppressed conductance where the charge configuration on the dot is fixed.

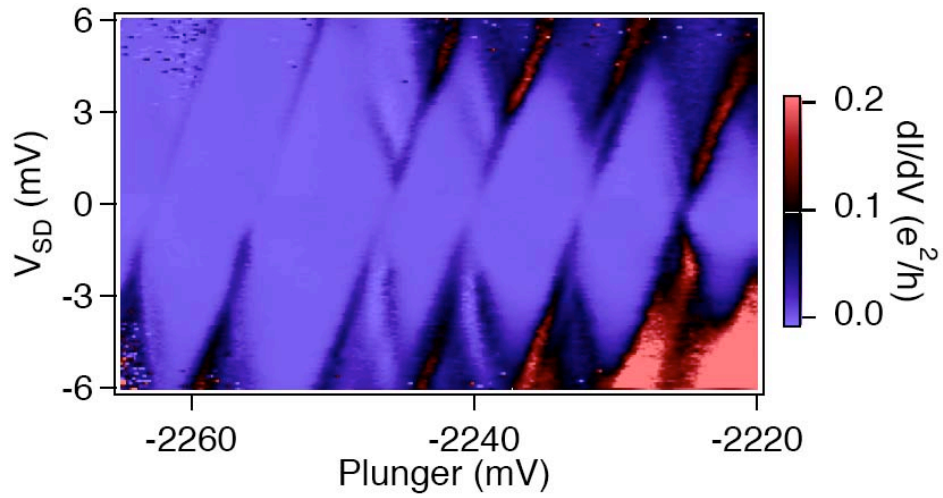


Figure 3. Coulomb diamonds measured on a device using ALD Al_2O_3 as the gate dielectric for $T \sim 270$ mK. Excited states are visible outside of the diamonds as off-resonance conduction is small in devices coated with ALD as opposed to PECVD. Gates were ~ 150 nm wide with ~ 150 nm spacing. Barrier 1 = -993 mV, Barrier 2 = -2337 mV, Backgate = 16 V. This device is strongly ambipolar, but is set into the electron-doped regime with the backgate.

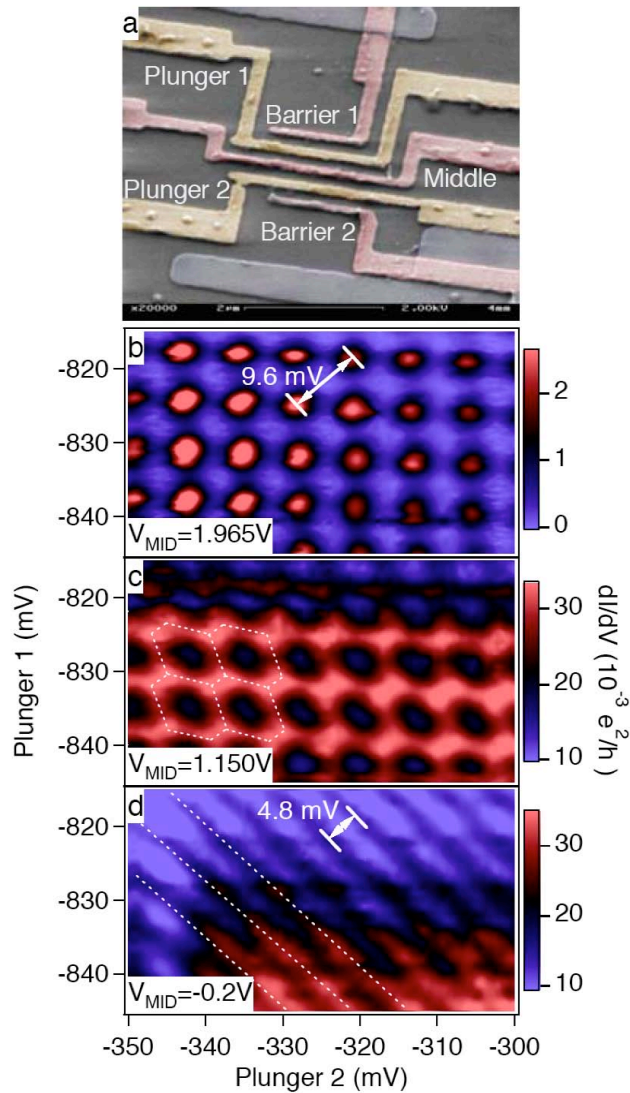


Figure 4a. False-color SEM image of a five-gate carbon nanotube device lithographically similar to that measured for this paper. Visible at top and bottom are Pd contacts to a nanotube (not visible) under SiO_2 . Gates used to form dots are red while plunger gates which tune dot energy levels are yellow. Scale bar = $2 \mu\text{m}$.

4b. dI/dV (colorscale) as a function of two plunger gate voltages. Barrier 1 = 389 mV, Barrier 2 = 1077 mV, Middle Gate voltage is indicated on the figure. Lockin excitation is $53 \mu\text{V}$. For the weak interdot coupling case, high conductance points appear on a regular array corresponding to resonant alignment of energy levels between the two dots with the Fermi levels of the leads. Note the low overall conductance.

4c. Intermediate interdot coupling case (lower middle gate voltage) in which charge interactions between the dots have led to a splitting of the original degeneracy points, and the formation of a honeycomb diagram. Dotted white lines serve as guides to the eye. Large off-resonance conductance along the honeycomb edges is due to higher order processes.

4d. Strongly coupled double dots (lowest middle gate voltage) behave as a large single dot with both plunger gates coupling equally to the single-particle states and producing a series of diagonal lines. Again, white dotted lines added as guides to the eye. Note the peak periodicity relative to the weakly coupled case in Fig. 4b.